Real-Time Monitoring of Molecular Dynamics of Ethylene Glycol Dimethacrylate Glass Former

M. T. Viciosa,*,†,‡ N. T. Correia,† M. Salmerón Sanchez,§,∥,⊥ A. L. Carvalho,† M. J. Romão,† J. L. Gómez Ribelles,§,∥,⊥ and M. Dionísio†

REQUIMTE, Departamento de Química, Faculdade de Ciências e Tecnologia da Universidade Nova de Lisboa, 2829-516 Caparica, Portugal, CQFM - Centro de Química-Física Molecular and IN - Institute of Nanoscience and Nanotechnology, Instituto Superior Técnico, Universidade Técnica de Lisboa, Avenida Rovisco Pais, 1049-001 Lisboa, Portugal, Centro de Biomateriales e Ingeniería Tisular, Universidad Politécnica de Valencia, Camino de Vera s/n, E-46022 Valencia, Spain, Centro de Investigación Príncipe Felipe, Avda. Autopista del Saler 16, 46013 Valencia, Spain, and CIBER en Bioingeniería, Biomateriales y Nanomedicina, Valencia, Spain

Received: April 7, 2009; Revised Manuscript Received: August 3, 2009

The isothermal cold-crystallization of the glass-former low-molecular-weight compound, ethylene glycol dimethacrylate (EGDMA), was monitored by real-time dielectric relaxation spectroscopy (DRS) and differential scanning calorimetry (DSC). The α-relaxation associated with the dynamic glass transition as detected by DRS was followed at different crystallization temperatures, T_{cr}, nearly above the glass transition temperature, 176 K ($1.06 \leq T_{cr}/T_g \leq 1.12$). It was found that the α-process depletes upon cold-crystallization with no significant changes in either shape or location. At advanced crystallization states, a new relaxation, α′-process, evolves that was assigned to the mobility of molecules lying adjacent to crystalline surfaces. From the time evolution of the normalized permittivity, it was possible to get kinetic information that was complemented with the calorimetric data. From DSC measurements that were also carried out under melt-crystallization, an enlarged temperature range was covered (up to $T_{cr}/T_g = 1.24$), allowing us to draw a diagram of time−temperature crystallization for this system. Dielectric relaxation spectroscopy proved to be a sensitive tool to probe the mobility in the remaining amorphous regions even at high crystallinities.

Introduction

In a previous work,[1] it was shown that ethylene glycol dimethacrylate (EGDMA), used as a cross-linking agent in dental restorative composites[2,3] and ophthalmic applications,[4,5] can be obtained as a fully amorphous glass or in a nearly fully crystalline state, depending on thermal treatment to which it is subjected. Crystallization was observed as occurring from both molten (melt-crystallization) and glassy (cold-crystallization) states.

It was observed that crystallization is easily avoided for *n*-ethyleneglycol dimethacrylates, with $2 \leq n \leq 4$, allowing us to classify these materials as molecular glass formers.[6,7] The respective dielectric characterization revealed, besides the α-relaxation process associated with the dynamical glass transition, two secondary relaxations, β and γ, on decreasing order of temperature. The dynamical behavior of EGDMA ($n = 1$) fits in the trend of their counterparts, finding that: (i) the onset of calorimetric glass transition increases with the number of ethylene glycol moieties ($T_g = 176$, 181, 187, and 190 K, respectively, for $n = 1$ to 4), the same happening with the α-process that shifts to higher temperatures with *n* increasing; (ii) the faster γ-process is independent of the size of the ethylene glycol group; and (iii) the β-relaxation slightly shifts to higher relaxation times with the increase of *n*.[1,7]

Due to the ability of EGDMA to crystallize, its real-time isothermal crystallization can be monitored by both differential scanning calorimetry (DSC) and dielectric relaxation spectroscopy (DRS). Both techniques were used to monitor isothermal cold-crystallization at several temperatures, T_{cr}, nearly above the glass transition temperature (T_{cr}/T_g within the range 1.06 to 1.12). Furthermore, DSC has been applied to follow the crystallization from the melt ($188 \text{ K} \leq T_{cr} \leq 218 \text{ K}$).

Usually, dielectric spectroscopy monitors isothermal crystallization through a reduction of the dielectric strength of the α-relaxation in either polymers like PET,[8,9] PLLA,[10–13] and polycarbonate/poly(ε-caprolactone) blends[14] or low molecular weight materials such as isooctyloxycyanobiphenyl[15] and triphenyl phosphite.[16] For EGDMA, with the progress of crystallization, the α-process depletes with no significant changes either in position or in shape.[1] A similar behavior is reported for the time evolution of the α-relaxation during crystallization in other low molecular weight materials, namely, isooctyloxycyanobiphenyl[15] and pharmaceutical drugs.[17,18] Nevertheless, the invariance in the peak position under crystallization is not universal, e.g., in sorbitol.[19] In a terephthalic acid dipropyl ester,[20] changes in peak position are reported to lower frequencies, while in 2-propanol a shift to higher frequencies (at crystallinities lower than 80%)[21,22] and to lower frequencies from 80% onward has been observed.[22]

It was found previously[1] that another relaxation process evolves in the low-frequency flank of the EGDMA α-peak, designated α′, when advanced crystallization stages are attained. The appearance of the α′-relaxation process is common in semicrystalline polymers being attributed to the relaxation of a

* Corresponding author. E-mail: teresaviciosa@ist.utl.pt.
† Faculdade de Ciências e Tecnologia da Universidade Nova de Lisboa.
‡ Universidade Técnica de Lisboa.
§ Universidad Politécnica de Valencia.
∥ Centro de Investigación Príncipe Felipe.
⊥ CIBER BBN.

10.1021/jp903212g CCC: $40.75 © 2009 American Chemical Society
Published on Web 10/05/2009

highly confined amorphous fraction located within the spherulites and on their surfaces: a rigid amorphous region.[8,9,12,13,23–26] Thus, semicrystalline polymers are usually considered as three phase systems: a more mobile amorphous region, a constrained amorphous fraction, and a crystalline phase. Although low molecular weight materials have different crystal morphology and crystal growth, under certain conditions, the evolving of a new relaxation process is also reported upon isothermal crystallization, e.g., sorbitol[19] and terephthalic acid dipropyl ester.[20]

The present work envisages being a further contribution concerning crystallization behavior of low molecular weight glass formers. Moreover, the kinetics of isothermal crystallizations will be analyzed. The kinetic behavior is often investigated by the classical Avrami law[27] which, in a double logarithmic plot, linearizes the time dependence of the crystallinity degree. However, such a plot does not hold for the entire range, and deviations from linearity are observed at longer times attributed to crystal impingement affecting the rate of crystal growth.[28–30]

Therefore, the direct fit to the normalized real dielectric permittivity, $\varepsilon'_N(t)$, provided by DRS and of the normalized enthalpy extracted from DSC, will be used to describe the crystallization kinetics of EGDMA, allowing us to extract several parameters as the constant rate, k, and the characteristic time, τ_{cr}, for crystallization taking as start values the ones found by the approach recently proposed by Avramov et al.[31] This data analysis also takes in account the induction time for crystallization, t_0, being more sensitive to changes in the time scale of τ_{cr}.[32]

EGDMA, which shows simultaneously a high intense dielectric α-relaxation and propensity to crystallize, proved to be a good candidate to study the crystallization process through the mobility of the coexistent amorphous fraction.

Experimental Section

Materials. Ethylene glycol dimethacrylate (EGDMA) with structure:

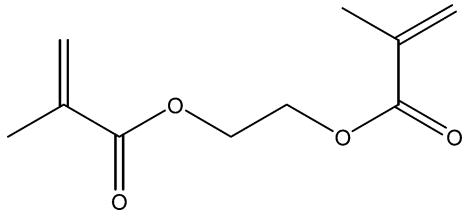

was supplied by Aldrich, cat. nbr. 33,568-1, MW = 198.22, 98% assay, and used as received. The purity of the compound was verified by ^{1}H NMR revealing the presence of only dimethacrylate-substituted ethyleneglycol, with no evidence of byproducts.[1] EGDMA has an intense dielectric response due to its large dipole moment, 5.3−5.4 D, as estimated for the isolated molecule.[33]

Dielectric Relaxation Spectroscopy. Dielectric measurements were carried out using the ALPHA-N impedance analyzer from Novocontrol GmBH. A drop of EGDMA was placed between two gold-plated electrodes (diameter 20 mm) of a parallel plate capacitor, BDS 1200, with two silica spacers, 50 μm thick. The sample cell was mounted on a cryostat, BDS 1100, and exposed to a heated gas stream being evaporated from a liquid nitrogen Dewar. The temperature control is assured by the Quatro Crysosystem and performed within ± 0.5 K. Novocontrol supplied all these modules.

To monitor isothermal cold-crystallization, the sample was previously cooled from room temperature to 153 K at 11 K·min^{-1}. The respective isochronal plots of both ε' and ε'' allowed checking the status of the sample confirming that no crystallization occurred. The ε' trace is especially sensitive to crystallization showing a marked fall due to the transformation from isotropic liquid to crystal.[34,35] No such feature was found during the cooling runs; an illustrative plot is shown in ref 1.

Then, the sample was rapidly heated to the cold-crystallization temperature, T_{cr}, (187, 189, 191, 193, 195, and 197 K) to avoid the growth of crystals. At T_{cr}, successive frequency sweeps from 0.7 Hz to 1 MHz were collected every 90 s during two hours (for T_{cr} = 187 K, the collection time was extended to 4 h due to the observed slowness of crystallization). Between different isothermal crystallization measurements, the sample was heated to 298 K, deeply in the molten state, to erase its thermal history and eliminate all crystalline nuclei.

X-ray Diffraction. The isothermal cold-crystallization at 193 K was also monitored by X-ray diffraction. An Enraf-Nonius X-ray generator with copper anode (Cu Kα X-ray radiation) and a graphite monochromator were used. The rotating anode generator was operating at 4.5 kW. An imaging plate (a mar300 system from MAR-Research) was used as an X-ray detector. The EGDMA sample was placed in a nylon loop (1.0 × 0.6 mm) and cooled to 153 K at a rate of 6 K·min^{-1} and then heated to 193 K at a heating rate of 6 K·min^{-1}. X-ray diffraction patterns were collected every 12 min while the sample was kept at 193 K during 3 h. The sample was submitted to an X-ray exposure time of 10 min while rotating 360° in a direction perpendicular to the X-ray beam, during each scan.

Differential Scanning Calorimetry. DSC was performed using a Perkin-Elmer Pyris 1 apparatus (melt crystallization experiments) and a Mettler 823E (cold crystallization). Temperature was calibrated by using zinc and indium. The melting heat of indium was used for calibrating heat flow.

To monitor isothermal cold-crystallization, the sample was cooled from 298 to 153 K at 20 K·min^{-1}, allowing for equilibration, and then the temperature jumped to the crystallization temperature, T_{cr} (exactly the same six temperatures tested by DRS were monitored by DSC). In the isothermal crystallization from the melt experiments, the sample was cooled at 20 K·min^{-1} from 298 K to the crystallization temperature T_{cr} (188, 193, 198, 203, 208, 213, 218, 218.6, 219, and 223 K), and the heat flow was recorded isothermally as a function of time.

Results

X-ray Diffraction. Figure 1 shows snapshots of X-ray diffraction patterns collected at several different crystallization times at 193 K. At t_{cr} = 0 min, only the amorphous halo is observed confirming that the sample is in the supercooled state. The sample in the nylon loop is totally transparent. Debye−Scherrer rings emerge as crystallization is occurring, which are clearly visible in the image taken at 28 min (second image from the top). The number and definition of the rings increases with the progress of crystallization. After 2 h, no more changes were observed in the diffraction patterns. The evolving of the Debye−Scherrer rings is in reasonable agreement with the observed decrease of the dielectric permittivity at T_{cr} = 193 K as described next.

Real-Time Dielectric Measurements during Cold-Crystallization. Figure 2 shows the real-time evolution of the dielectric loss during the isothermal cold-crystallization process for the six different temperatures studied. The respective real part (not shown) in the low frequency range is frequency independent, which can be taken as an indication that each frequency sweep is carried out in a time short enough to preserve the sample in

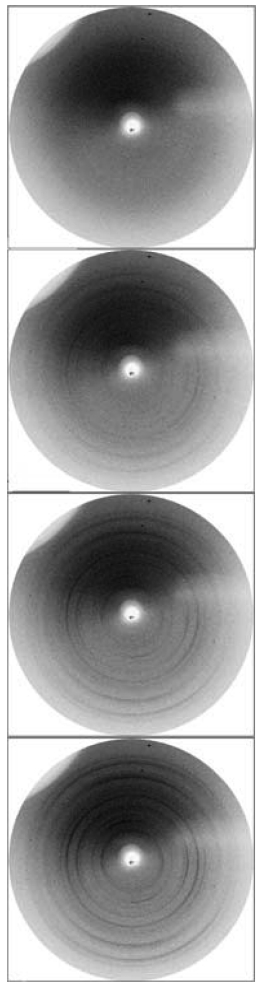

Figure 1. Snapshots of X-ray diffraction pattern at 193 K upon isothermal cold-crystallization taken at different crystallization times. From the top: 0, 28, 73, and 120 min; after 120 min no further changes were observed.

an isostructural state.[17] The insets present the time dependence of the real permittivity at 1 Hz.

At the earliest stages of crystallization, all spectra exhibit an intense α-peak associated with the dynamical glass transition, however, being influenced by the secondary γ-process in the high frequency flank. While crystallization progresses, three main features are observed: (i) the intensity of the α process reduces with the increase of crystallization time concomitantly with a decrease in the increment of the real part of the complex permittivity (not shown); (ii) the α peak does not show any significant changes in either position or shape; and (iii) for $T_{cr} \geq 191$ K, at high crystallization degrees another relaxation process evolves in the low frequency flank of the α-peak, designated as α′. Under certain conditions when crystallization is carried out at 193 K, the β-relaxation can also persist with the α′-process after the complete extinction of the α-relaxation as reported in ref 1.

To analyze the dielectric response in more detail, the model function introduced by Havriliak−Negami[36] was fitted to the experimental data. Because multiple peaks are observed in the available frequency window, a sum of HN-functions is employed

$$\varepsilon^*(f) = \varepsilon_\infty + \sum_j \frac{\Delta\varepsilon_j}{[1 + (i\omega\tau_{HN})^{\alpha_{HNj}}]^{\beta_{HNj}}} \quad (1)$$

where j is the index over which the relaxation processes are summed; $\Delta\varepsilon$ is the dielectric strength; τ_{HN} is the characteristic HN relaxation time; and α_{HN} and β_{HN} are fractional parameters ($0 < \alpha_{HN} \leq 1$ and $0 < \alpha_{HN}\beta_{HN} \leq 1$) describing, respectively, the symmetric and asymmetric broadening of the complex dielectric function.[37]

For crystallization carried out at $T_{cr} \geq 191$ K, eq 1 was fitted to the dielectric spectra considering three relaxations: (i) the main relaxation, which is the major contribution in the first crystallization times, (ii) the γ-relaxation that becomes important when the α-relaxation is significantly depleted, and (iii) the relaxation located in the low frequency side of the α-process identified as α′. After several tentative fitting analyses, it was concluded that during isothermal crystallization only the dielectric strength of the three relaxations and the α_{HN} shape parameter of the α-process change; the fixed parameters for each T_{cr} are summarized in Table 1. Figure 3 illustrates the time dependence of $\Delta\varepsilon$ for the three considered processes for crystallization carried out at 197 K.

While for crystallization temperatures above 193 K the α-peak is completely extinguished, it persists when crystallization is carried out at lower temperatures. At 189 and 187 K, the slower evolution of crystallization did not allow observing the emergence of the third process, and consequently, only two HN were considered in the data treatment.

The variation of the reduced dielectric strength $\Delta\varepsilon_\alpha$ with the crystallization time can be used to estimate the crystallinity degree (χ_{cr}), considering that the relaxation intensity is proportional to the amount of noncrystalline phase.[34] Thus, the time dependence of the degree of crystallinity for $T_{cr} < 193$ K was estimated from the normalized dielectric strength according to[17,20,22]

$$\chi_{cr}(t) = 1 - \frac{\Delta\varepsilon_\alpha(t)}{\Delta\varepsilon_\alpha(t=0)} \quad (2)$$

Since, for $T_{cr} \geq 191$ K a third process is detected, the dielectric strength of the remaining amorphous phase should account for the contribution of both bulk-like (α-process) and constrained (α′-process) amorphous fractions. Several authors have shown that this process, mainly observed in polymers, as mentioned in the Introduction, should be taken into account through $\Delta\varepsilon_{\alpha+\alpha'}$ to agree with the structural development evaluated by the magnitude of properties estimated independently such as SAXS and WAXS,[14,38] WANS,[39] and the reduced intensity of the secondary β-process.[40] Therefore, $\Delta\varepsilon_{\alpha+\alpha'}$, shown in Figure 4a, describes more properly the global crystallization process and consequently the decrease of total amorphous region, being the quantity considered to estimate the crystallinity degree, χ_{cr}, in eq 2.

The time dependence of the crystallinity degree, χ_{cr}, is shown in Figure 4b (full circles). It attains a value close to unity for the four highest temperatures. A value near below 0.6 is reached for $T_{cr} = 189$ and 187 K; however, in the latter, a crystallization time two times longer was necessary to achieve the same value of χ_{cr} (not shown).

Alternatively, the progress of crystallization can be analyzed from the normalized real permittivity[15,32,34]

$$\varepsilon'_N(t) = \frac{\varepsilon'(0) - \varepsilon'(t)}{\varepsilon'(0) - \varepsilon'(\infty)} \quad (3)$$

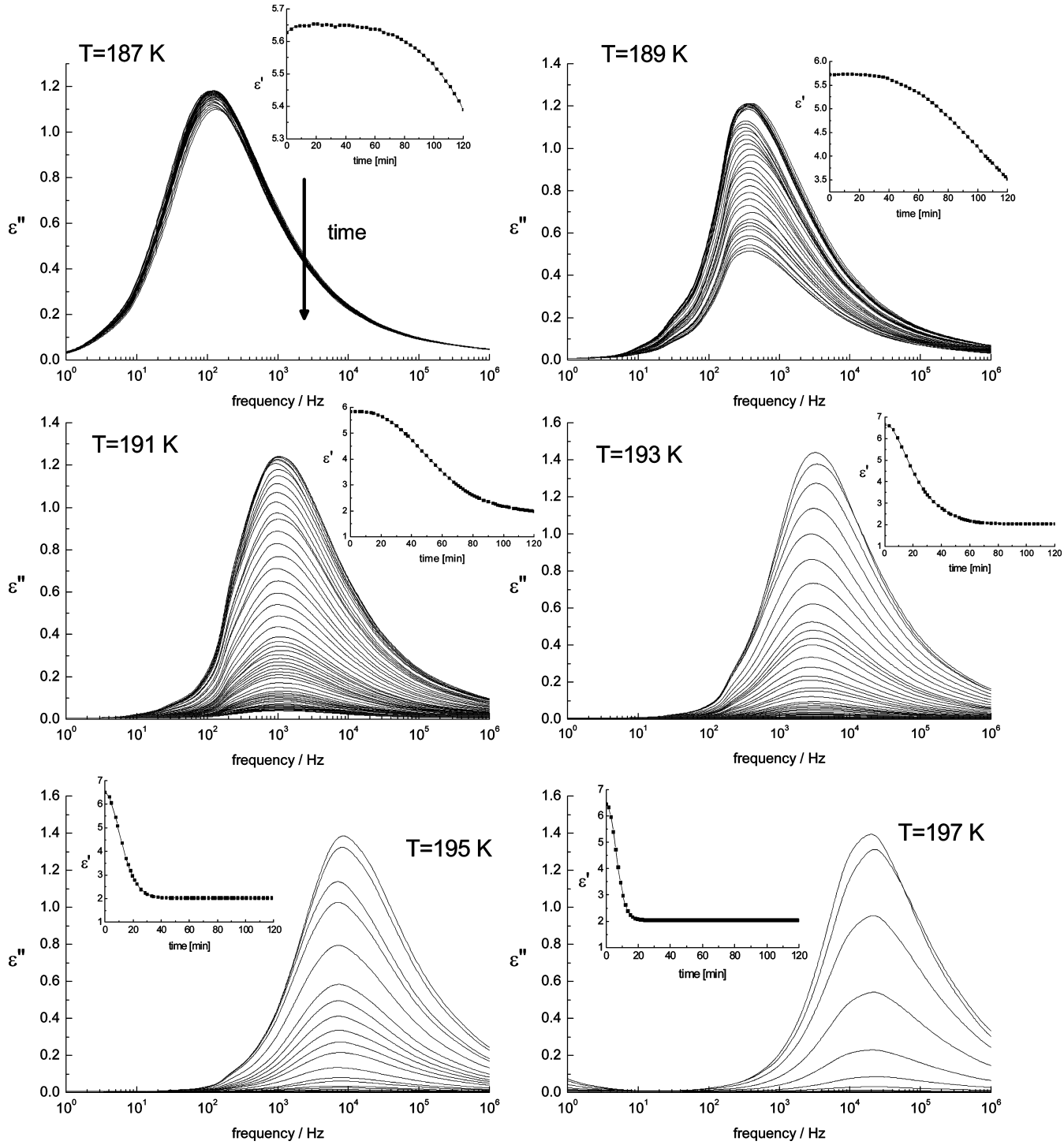

Figure 2. Real-time DRS monitoring of EGDMA isothermal cold-crystallization carried out at different temperatures during 2 h: the illustrated dielectric loss spectra were collected every 3 min. Inset: Time evolution of the real permittivity at 1 Hz during crystallization.

where $\varepsilon'(0)$ is the dielectric permittivity at the start of the crystallization; $\varepsilon'(\infty)$ is the long time limiting value; and $\varepsilon'(t)$ is the value at the allowed time for crystallization, t. Since ε'_N is independent of a model function, the good agreement observed between ε'_N and χ_{cr} (see Figure 4b) can be taken as a validation of the way the HN function was fitted to the complex permittivity. Figure 4c is the semilogarithmic plot of ε'_N that will be analyzed later.

A widespread treatment in the literature to analyze the transformation from the disordered amorphous into the ordered crystalline phase at a fixed temperature is the Avrami model.[27,41,42] In this treatment of the isothermal crystallization kinetics, different nucleation and growth mechanisms have correspondingly different time dependences of the crystallization rate that can be modeled by the Avrami law,[27] which in terms of ε'_N reads

$$\varepsilon'_N(t) = 1 - \exp(-kt^n) \quad (4)$$

where k is a temperature-dependent rate constant and n is the Avrami parameter that can take values between 1 and 7 depending on nucleation type and crystal growth mechanism.[15,33,43] A plot of $\ln[-\ln(1 - \varepsilon'_N(t))]$ vs $\ln t$ (linearization of eq 4) is shown in Figure 5 for all tested temperatures. As mentioned previously in the

TABLE 1: HN Fitting Parameters That Were Fixed during the Fitting Procedure of Data Corresponding to the Isothermal Cold-Crystallization of EGDMA at the Crystallization Temperatures T_{cr} Indicated Inside[a]

	α				α′			γ			
T_{cr} [K]	α_{HN}	β_{HN}	τ_{HN}/s		α_{HN}	β_{HN}	τ_{HN}/S	α_{HN}	β_{HN}	τ_{HN}/s	
187	0.95	0.49	2.5	10^{-3}	–	–	–	0.42	0.44	7.3	10^{-5}
189	0.95	0.48	8.1	10^{-4}	–	–	–	0.42	0.44	5.5	10^{-5}
191	0.95	0.48	2.8	10^{-4}	0.23	1.00	1.33	0.42	0.44	4.0	10^{-5}
193	0.96	0.45	1.1	10^{-4}	0.22	1.00	0.93	0.42	0.44	3.1	10^{-5}
195	0.96	0.47	4.0	10^{-5}	0.21	1.00	0.65	0.42	0.44	2.3	10^{-5}
197	0.96	0.47	(1.3 ± 0.3)	10^{-5}	0.24	1.00	0.46	0.42	0.44	1.8	10^{-5}

[a] For T_{cr} = 193 and 195 K, a reasonable fit was only achieved when the α_{HN} parameter was allowed to vary within the indicated limits.

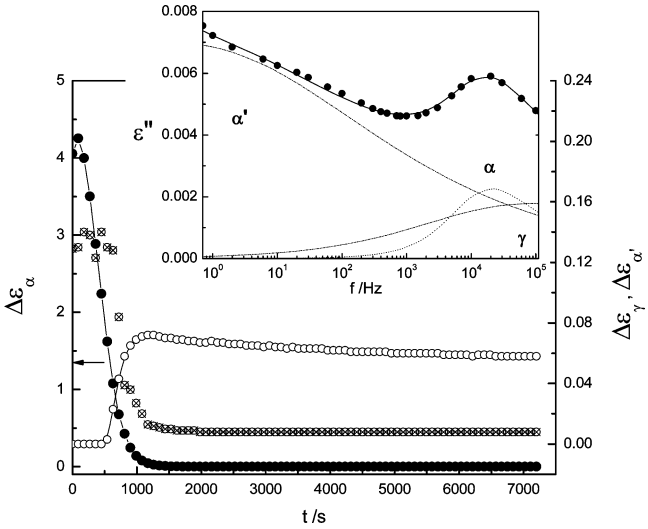

Figure 3. Time dependence of the dielectric strength obtained by fitting a sum of HN functions to the data during isothermal cold-crystallization at 197 K: filled circles correspond to the α-relaxation (left axis) and open circles to α′- and crossed circles to γ-process (right axis). Lines are guides for the eyes. In the inset, the spectrum collected after 24 min of crystallization at 197 K is shown: individual HN functions are represented as dotted lines and the overall HN fit as a solid line.

Introduction, the Avrami plot does not hold for the entire time range: data concerning the highest temperatures at which isothermal crystallization was monitored reveal a change of slope, the flat region at longer times corresponding to an invariant crystallization degree achieved.

The Avrami equation can be rewritten taking in account t_0, the induction time preceding crystallization and a characteristic time for the isothermal crystallization, τ_{cr}[27,31,44]

$$\varepsilon'_N(t) = 1 - \exp\left[-\left(\frac{t - t_0}{\tau_{cr}}\right)^n\right] \quad (5)$$

where $\varepsilon'_N(t)$ is the fraction transformed in the crystalline phase at time (t) and τ_{cr} is obtainable from the Avrami parameters by the relationship $\tau_{cr} = k^{-1/n}$. Equation 5 is the basis of a modified method of data analysis proposed by Avramov et al.[31] which is more sensitive to the changes in the time scale of τ_{cr}, avoiding problems due to a noncorrect evaluation of t_0 or lack of thermal stability in collecting the first experimental points.[32]

To estimate τ_{cr}, eq 5 was directly fitted to $\varepsilon'_N(t)$ data having also as fitting parameters t_0 and n; for iteration, the starting values of t_0 and n were obtained graphically according the modified Avramov analysis.[31,32] In Figure 4b, it is shown as solid lines how $\varepsilon'_N(t)$ (full circles) is well described by eq 5 in all time ranges, and Figure 4c enhances the agreement obtained for the shortest times in a semilogarithmic plot, being especially sensitive to the value of the induction time. The estimated quantities are included in Table 2. In general, it is observed that t_0 and τ_{cr} increase with decreasing T_{cr} which will be analyzed in more detail later, and n presents slightly higher values for the lowest temperatures.

Calorimetric Studies. To allow a comparison with dielectric experiments, cold crystallization isotherms were recorded by DSC. Figure 6a shows the respective cold crystallization thermograms.The integration of the experimental thermograms allowed calculating the normalized crystallization enthalpy ($\Delta h_{cr}(t)/\Delta h_{cr}(t=\infty)$), as a function of crystallization times (inset of Figure 6a). This quantity corresponds to the fraction transformed in the crystalline phase at time (t), allowing an identical analysis as done for DRS (eq 5). The solid lines in the inset of Figure 6a represent the model calculated curves for which corresponding Avrami parameters are listed in Table 3.

Isothermal crystallization from the melt conducted between 188 and 223 K was also followed calorimetrically; at 219 and 223 K no crystallization peak was detected during 200 min of measurement (the heat flow was constant over this period). Only some of the curves collected below 219 K are shown in Figure 6b for clarity. The exothermal heat flow against time shows a symmetric peak (as found in cold-crystallization) in the temperature range between 188 and 213 K, but above this temperature the shape of the exotherm is quite irregular. The time of the onset of melt-crystallization (t_{onset}), i.e., at which the peak shows up, shifts toward lower times between 188 and 213 K, and then starts increasing again up to 218.6 K as shown in the inset of Figure 6b. The plot evidences the existence of a minimum, i.e., maximum crystallization rate at around 213 K.

The crystallization exotherm from the cold-crystallization recorded at 193K (curve c) is included in Figure 6b to allow a comparison. This exothermal peak appears slightly shifted toward shorter times with respect to melt-crystallization (curve m) due to nucleation taking place in the former during cooling to 153 K previous to the isothermal crystal growth. The position of the onset of cold-crystallization curves is included in the inset of Figure 6b.

After each isothermal treatment, a heating scan at 10 K·min^{-1} was recorded showing the melting peak with a shape and location independent of the crystallization temperature (T_{onset} = 264.8 K; T_{peak} = 271.2 K). The melting endotherm peak was only detected for those temperatures in which crystallization occurred in the previous isothermal treatment.The crystallization enthalpy increments, Δh_{cr}, are presented in Table 4.

Data corresponding to crystallization at 208 K were not included since the respective exotherm was not complete due to the lack of heat flow stabilization before the onset of crystallization making very uncertain the integration of the peak.

Discussion

The isothermal crystallization of the EGDMA glass former was monitored by both DRS and DSC techniques. The obtained

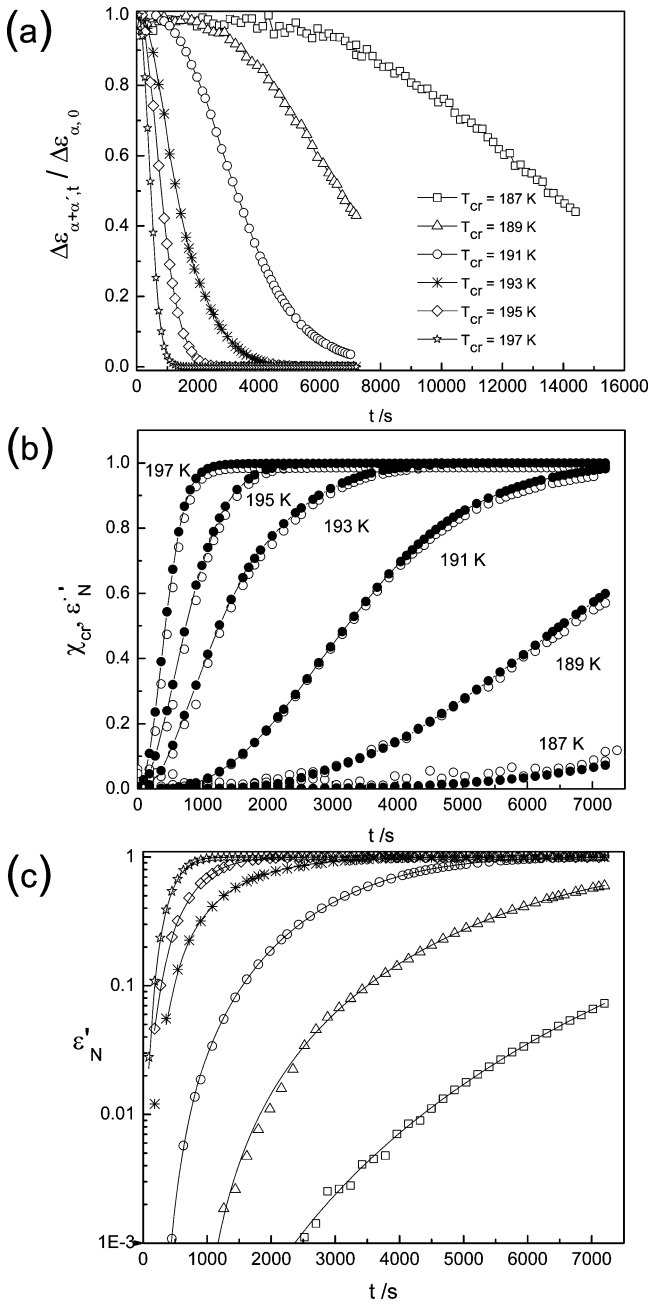

Figure 4. (a) Time evolution of the dielectric strength, $\Delta\varepsilon_{\alpha+\alpha',t}$, for the amorphous fraction (mobile (α) and rigid (α′)), normalized by the value measured for the complete amorphous state $\Delta\varepsilon_{\alpha,0}$ (intensity of the α-relaxation observed for crystallization time $t = 0$). Cold-crystallization at 187 K was followed during 4 h. For $T_{cr} < 193$ K, the α′-process was not observed, thus $\Delta\varepsilon_{\alpha+\alpha',t} \equiv \Delta\varepsilon_{\alpha,t}$, the dielectric strength of α-relaxation (for more details see text). (b) Time dependence of the crystallinity degree, χ_{cr} (open circles), estimated from the dielectric strength (eq 2) and normalized real permittivity, ε'_N (full circles). Solid lines are fits to ε'_N data using eq 5. (c) Semilogarithmic plot of ε'_N in function of time evidencing how well eq 5 describes data for the initial times and its sensitivity to the induction time.

results demonstrate that EGDMA is able to crystallize from both glassy and molten states. X-ray patterns confirmed the occurrence of cold-crystallization.

The magnitude of the α-relaxation continuously decreases upon isothermal crystallization without changing its position. This insensitivity of the relaxation time suggests that the domain size of the cooperative motion underlying the dynamic glass transition is sufficiently small relative to the distance between

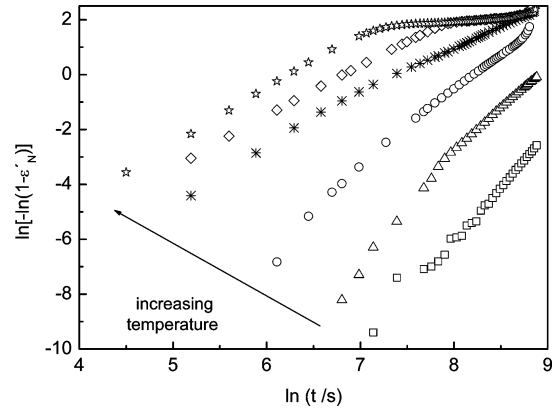

Figure 5. Avrami plot of the normalized real dielectric permittivity ε'_N for all the cold-crystallization temperatures reported in Figure 4.

TABLE 2: Kinetic Parameters Obtained from the Fit of Equation 5 to the Normalized Dielectric Permittivity Data, ε'_N, for the Cold-Crystallization Temperatures T_{cr}[a]

T_{cr}/K	t_0/s	τ_{cr}/s	n	k/s^{-n}
187	1430 ± 274	13700 ± 200	3.0 ± 0.2	3.89×10^{-13}
189	855 ± 46	6660 ± 43	2.48 ± 0.02	3.28×10^{-10}
191	256 ± 61	3413 ± 65	2.31 ± 0.05	4.97×10^{-9}
193	138 ± 50	1459 ± 56	1.60 ± 0.07	1.36×10^{-5}
195	32 ± 3	879 ± 4	1.72 ± 0.01	2.85×10^{-5}
197	22 ± 8	487 ± 8	1.92 ± 0.04	1.15×10^{-5}

[a] k is the temperature-dependent rate constant that verifies the relation $\tau_{cr} = k^{-1/n}$.

crystallites, so the growing crystal units do not perturb dipole relaxation.[17,45] At advanced crystallization states, only achieved when $T_{cr} \geq 191$ K, a new process emerges in the low frequency flank of the α-process. This so-called α′-process is generally observed in semicrystalline polymers and some low molecular weight materials as mentioned in the Introduction.

In many crystallized polymers, the material may become 100% spherulitic; however, only a part is crystalline, so the amorphous fraction is constrained within the spherulites.[8,38] Therefore, during crystallization, the polymeric system evolutes as a three-phase system: a more mobile amorphous region, a constrained amorphous fraction, and a crystalline phase. In the case of low molar mass systems, as here reported, the material attains very high crystallinity degrees being unlikely that at the end of crystallization a bulk constrained amorphous part could exist within the crystallites; therefore, the relaxation detected should be associated to the mobility of molecules lying adjacent to crystalline surfaces.

Experimental evidence of this interface between crystals is not as straightforward as in semicrystalline polymers where the existence of a bulk rigid amorphous phase is established by a reduction in the incremental step change in the heat capacity at T_g compared to what would be expected to the measured crystalline degree, the latter determined independently.[46] Nevertheless, in the crystallized low molecular weight terephthalic acid dipropyl ester,[20] a small amorphous fraction (2%) remains after long-time crystallization, able to be detected by both DSC and DRS revealing a shift of the glass transition to higher temperatures; moreover, since the whole noncrystalline part participates in the relaxation process, the authors found that the system could be well described by the two-phase model. The behavior was assigned to spatial confinement of the amorphous interface between the lamellae-like crystals where a molecule is unable to incorporate by sterical hindrance in a neighboring crystal.

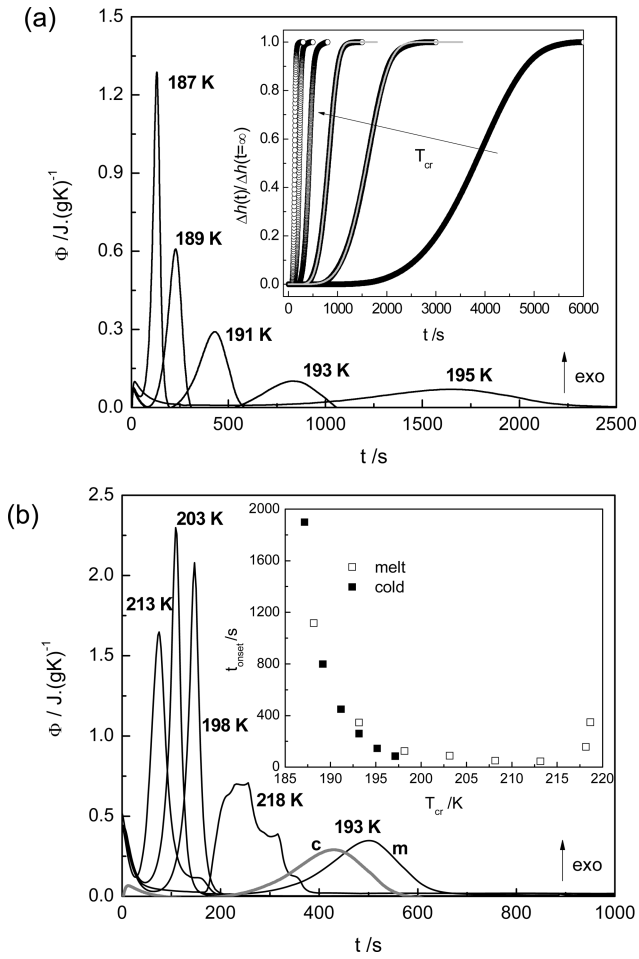

Figure 6. (a) DSC crystallization isotherms (heat flow versus crystallization time, t) of EGDMA cold-crystallized at several temperatures T_{cr}. The inset presents the normalized crystallization enthalpy ($\Delta h_{cr}(t)/\Delta h_{cr}(t=\infty)$), as a function of crystallization time, at each T_{cr} and illustrates the fit of the modified Avrami function for $T_{cr} = 191$ and 189 K (gray lines). (b) DSC crystallization isotherms of EGDMA melt-crystallized at several temperatures. Lines c and m refer to cold and melt crystallizations carried at 193 K. The inset shows the time of the onset of the isothermal melt- (open squares) and cold-crystallization peaks, obtained from DSC measurements, as a function of crystallization temperature (T_{cr}).

TABLE 3: Crystallization Enthalpy (Δh_{cr}) and Kinetic Parameters Obtained from the Fit of Equation 5 to the Normalized Crystallization Enthalpy for the Cold-Crystallization Temperatures T_{cr}[a]

T_{cr}/K	Δh_{cr}/kJ·mol^{-1}	t_0/s	τ_{cr}/s	n	k/s^{-n}
187	10.0	398 ± 8	3688 ± 8	4.4 ± 0.1	1.58×10^{-16}
189	11.5	178 ± 6	1537 ± 6	4.4 ± 0.1	1.02×10^{-14}
191	10.4	172 ± 3	693 ± 3	4.4 ± 0.1	2.78×10^{-13}
193	11.4	142 ± 4	306 ± 4	3.9 ± 0.1	8.31×10^{-13}
195	11.5	54 ± 4	181 ± 4	4.6 ± 0.1	4.12×10^{-11}
197	11.5	51 ± 2	84 ± 2	4.2 ± 0.1	8.66×10^{-9}

[a] k is the temperature-dependent rate constant that verifies the relation $\tau_{cr} = k^{-1/n}$.

It is worthwhile to mention that the relaxation strength in crystallized EGDMA is reduced to much less than 1% of the original α-process intensity (around 200 times) revealing much higher crystallinity as compared with the above-mentioned low molecular weight material, being unlikely that the remaining noncrystalline fraction be detected/characterized by other means. Nevertheless, the dielectric strength of both α- and α′-processes was taken into account while estimating the degree of crystallinity.

TABLE 4: Crystallization Enthalpy (Δh_{cr}) and Kinetic Parameters Obtained from the Fit of Equation 5 to the Normalized Crystallization Enthalpy for the Melt-Crystallization Temperatures T_{cr}[a]

T_{cr}/K	Δh_{cr}/kJ·mol^{-1}	t_0/s	τ_{cr}/s	n	k/s^{-n}
188	11.5	400 ± 76	2843 ± 78	4.5 ± 0.1	2.87×10^{-16}
193	12.0	150 ± 16	362 ± 14	4.9 ± 0.2	2.90×10^{-13}
198	12.8	325 ± 37	125 ± 38	7 ± 2	2.10×10^{-15}
203	13.7	312 ± 17	86 ± 17	5 ± 1	2.13×10^{-10}
213	14.3	255 ± 17	85 ± 17	4 ± 1	1.92×10^{-8}

[a] k is the temperature-dependent rate constant that verifies the relation $\tau_{cr} = k^{-1/n}$.

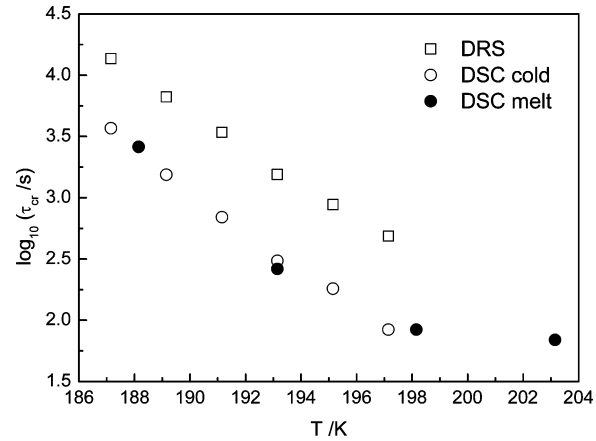

Figure 7. Temperature dependence of τ_{cr} obtained from the Avrami model fit to dielectric data ($\tau_{cr,DRS}$, open squares) and to DSC data: cold-crystallization ($\tau_{cr,DSC}$, open circles) and melt-crystallization (filled circles).

The systematic decrease of the normalized dielectric permittivity at a single frequency and the ratio $\Delta h_{cr}(t)/\Delta h_{cr}(t=\infty)$ were used to compute the crystallization kinetics from dielectric and DSC experiments, respectively. Both properties were fitted with a modified Avrami equation allowing extracting the induction time, t_0, the time for crystallization, τ_{cr}, and the Avrami parameter n. Table 2 summarizes the fitting parameters obtained by DRS, and Tables 3 and 4 present the respective parameters obtained from DSC data from, respectively, cold- and melt-crystallization.

The crystallization process is faster in DSC than in dielectric experiments, a fact that must be ascribed to the different geometry of the sample holders in both techniques. In the dielectric cell, the liquid was allocated in a thin layer of around 50 μm between the electrodes, while in DSC, although the sample mass is small, the thickness of the layer is larger. The difference in the crystallization behavior of EGDMA between the two techniques was also found in a previous work under the same temperature protocols.[1]

While the estimated induction time for cold-crystallization, in the studied temperature interval, increases with a decrease in temperature, for melt-crystallization that covers a more extended temperature range, and t_0 generally follows the temperature dependence observed for the experimental time of onset for crystallization shown earlier in the inset of Figure 6b.

The temperature dependence of the estimated time for crystallization, τ_{cr}, is shown in Figure 7. The fact that, in the temperature range of the dielectric experiments, crystallization rate increases with the temperature increase, as also seen by the augment of k with T_{cr} increase (Tables 2, 3, and 4), means that both cold- and melt-crystallization are dominated by the

diffusion of molecules that control crystal growth rather than nucleation, for which the rate would decrease with increasing T_{cr}.[34]

DSC allows a comparison of the kinetics of cold- and melt-crystallization. The higher crystallization rate of cold-crystallization compared to melt can be attributed to the formation of additional nuclei during previous undercooling in the former since the nucleation rate increases with decreasing temperature. Thus, in cold crystallization, most of the crystallization nuclei already exist at the beginning of the crystallization process.

Concerning the estimation of n that plays a key role for the kinetics of the crystallization process accounting for the dimensionality of crystal growth, eq 5 was directly fitted to the time-dependent normalized real permittivity and crystallization enthalpy. This procedure diminishes the importance of the contribution of the initial stages as well as that of the stages near the end of the process that in the conventional double logarithmic Avrami's plot are exaggerated going to infinity. No significant differences were found in the n parameter determined for cold- or melt-crystallization by DSC with values between 4 and 5, in general. On the other hand, dielectric data were well-represented by low Avrami exponents, which in light of the model could be interpreted as a crystal growth of low dimensionality. Nevertheless, such low n values were also estimated from dielectric data for other glass-former systems,[14,15,28,34] even when complementary techniques, such as optical microscopy, show the formation of spherulites compatible with higher n values predicted by the Avrami theory.[14,34]

Some authors[14] claim that the transformation process is rather complex involving simultaneously crystallization and formation of a rigid amorphous fraction, the latter confirmed by the existence of the α′-process as observed for EGDMA, and therefore, the crystallization description by a simple kinetic treatment such as the Avrami model could be inappropriate. We also note that the n values obtained for EGDMA from dielectric results are lower than those derived from the calorimetric measurements, the latter consistent with a crystal growth of higher dimensionality; nevertheless, the sample geometry used in those techniques is different which could also affect the growth mechanism as already mentioned. Therefore, complementary information is needed to reach a conclusion about the geometry of the growth.

With respect to the crystallization degree attained, it is difficult to establish if the full crystalline state was achieved by DSC. The crystallization enthalpy decreases with undercooling below the melting point, $T_m - T_{cr}$, and is always lower than the melting enthalpy ($\Delta h_m = 20.2 \pm 0.6$ kJ·mol^{-1}).[1] The reason for that is obviously the temperature dependence of the enthalpy of the liquid and the solid according to their respective heat capacity c_{pl} and c_{ps}. Thus, assuming that the difference $\Delta c_p = c_{pl} - c_{ps}$ is independent of temperature, the enthalpy increment of the crystallization at temperature T_{cr} can be written

$$|\Delta h_c(T_{cr})| = h_l(T_{cr}) - h_s(T_{cr}) = h_l(T_m) - h_s(T_m) - (c_{pl} - c_{ps})(T_m - T_{cr}) \quad (6)$$

T_m being the equilibrium melting temperature. Equation 6 explains the linear dependence of Δh_{cr} with temperature and allows determining $\Delta c_p = c_{pl} - c_{ps}$ from the experimental results, obtaining a value of $\Delta c_p = c_{pl} - c_{ps} = 138.6$ J·(K·mol)$^{-1}$, slightly higher than the heat capacity difference between the liquid and the glass ($\Delta c_p(T_g) = 114.9$ J·(K·mol)$^{-1}$ determined in heating scans).[1] The fit of eq 6 to the experimental values yields $h_l(T_m) - h_s(T_m) = 21.4$ kJ·mol^{-1}, close to the values determined by integration of the melting endotherms detected during the heating scans; however, it can not be unambiguously concluded that complete crystallization from the melt was attained as probed by DSC.

Concerning cold-crystallization, dielectric results showed that even when it was promoted at the highest temperatures ($T_{cr} \geq 193$ K), despite most of the material being almost in a full crystalline state, some residual mobility still persists occurring adjacent to the crystalline surfaces as revealed by the detection of the hindered α′-process.

The way the crystallinity degree is evaluated through the value of the dielectric strength assumes that only the effective dipole moment is changing due to crystallization. However, the density increases and the Kirkwood correlation factor, g, could also change due to extra correlations that establish under continuous crystallization, and thus the χ_{cr} values should be considered carefully. Even so, there is no doubt that elevated crystallinities were achieved as the vanishing of the α-process demonstrates being important to stress the sensitivity of dielectric relaxation spectroscopy that still probes the mobility in the amorphous regions when approaching so high crystalline degrees.

Conclusions

The isothermal crystallization of the low molecular weight glass-former EGDMA was followed in real-time by DRS and DSC.

The intense α-peak detected by dielectric relaxation spectroscopy associated with the dynamic glass transition was used to monitor the real-time isothermal cold-crystallization nearly at and above T_g (176 K). In general, no significant changes in either position or shape were detected in the α-peak upon crystallization in the first stages of crystallization. Furthermore, at high crystallization degrees achieved for crystallization temperatures above 193 K, a new relaxation process (α′) emerges in the low frequency flank of the α-peak, attributed to conformational mobility originated in the remaining amorphous fraction adjacent to the crystal surfaces.

The calorimetric data which covered a more extended temperature range for melt-crystallization allowed defining a time−temperature diagram where a maximum crystallization rate (minimum time onset for crystallization) was found close to 213 K.

The time evolution of both normalized dielectric permittivity and normalized crystallization enthalpy was analyzed by the Avrami model taking into account the induction time, t_0, allowing also extraction of the crystallization times, τ_{cr}, and the Avrami exponents, n. The decreasing of τ_{cr} with the temperature increase for $T_{cr} \leq 198$ K is compatible, in this temperature range, with a diffusion-controlled process in either cold- or melt-crystallization. The Avrami exponents estimated from dielectric data are low in contrast with the values found from calorimetric data. This discrepancy also observed by others could suggest an inadequacy of the Avrami model to describe the complexity of the crystallization process or a different crystal dimensionality due to different geometries of sample holders in DRS vs DSC.

Acknowledgment. The authors deeply acknowledge the helpful discussions with Prof. Graham Williams. Financial support to Fundação para a Ciência e Tecnologia (FCT, Portugal) is acknowledged through the project PTDC/CTM/64288/2006 and a postdoc grant SFRH/BPD/39691/2007 (M. T. Viciosa). J. L. Gómez Ribelles acknowledges the support of the Spanish Ministry of Science through project No. MAT2007-

66759-C03-01 (including the FEDER financial support) and funding for research in the field of Regenerative Medicine through the collaboration agreement from the Conselleria de Sanidad (Generalitat Valenciana) and the Instituto de Salud Carlos III (Ministry of Science and Innovation).

References and Notes

(1) Viciosa, M. T.; Correia, N. T.; Salmerón Sánchez, M.; Gómez Ribelles, J. L.; Dionísio, M. *J. Phys. Chem. B*, DOI: 10.1021/jp903208k.
(2) Bland, M. H.; Peppas, N. A. *Biomaterials* **1996**, *17*, 1109.
(3) Krishnan, V. K.; Manjusha, K.; Yamuna, V. J. *Mater. Sci.-Mater. Med.* **1997**, *8*, 703.
(4) Alvarez-Lorenzo, C.; Hiratani, H.; Gómez-Amoza, J. L.; Martínez-Pacheco, R.; Souto, C.; Concheiro, A. *J. Pharm. Sci.* **2002**, *91*, 2182.
(5) Chetoni, P.; Di Colo, G.; Grandi, M.; Morelli, M.; Saettone, M. F.; Darougar, S. *Eur. J. Pharm. Biopharm.* **1998**, *46*, 125.
(6) Viciosa, M. T.; Dionísio, M. *J. Non-Cryst. Solids* **2004**, *341*, 60.
(7) Viciosa, M. T.; Brás, A. R.; Gómez Ribelles, J. L.; Dionísio, M. *Eur. Polym. J.* **2008**, *44*, 155.
(8) Williams, G. *Adv. Polym. Sci.* **1979**, *33*, 59.
(9) Ezquerra, T. A.; Baltá-Calleja, F. J.; Zachmann, H. G. *Polymer* **1994**, *35*, 2600.
(10) Mijoviæ, J.; Sy, J. W. *Macromolecules* **2002**, *35*, 6370.
(11) Fitz, B. D.; Andjelić, S. *Polymer* **2003**, *44*, 3031.
(12) Dionísio, M.; Viciosa, M. T.; Wang, Y.; Mano, J. F. *Macromol. Rapid Commun.* **2005**, *26*, 1423.
(13) Brás, A. R.; Viciosa, M. T.; Wang, Y.; Dionísio, M.; Mano, J. F. *Macromolecules* **2006**, *39*, 6513.
(14) Laredo, E.; Graimau, M.; Barriola, P.; Bello, A.; Müller, A. J. *Polymer* **2005**, *46*, 6532.
(15) Massalska-Arodz, M.; Williams, G.; Thomas, D. K.; Jones, W. J.; Dabrowski, R. *J. Phys. Chem. B* **1999**, *103*, 4197.
(16) Hédoux, A.; Denicourt, T.; Guinet, Y.; Carpentier, L.; Descamps, M. *Solid State Commun.* **2002**, *122*, 373.
(17) Alie, J.; Menegotto, J.; Cardon, P.; Duplaa, H.; Caron, A.; Lacabanne, C.; Bauer, M. *J. Pharm. Sci.* **2004**, *93*, 218.
(18) Rengarajan, G. T.; Beiner, M. *Lett. Drug Des. Discovery* **2006**, *3*, 723.
(19) Minoguchi, A.; Nozaki, R. *J. Non-Cryst. Solids* **2002**, *307−310*, 246.
(20) Dobbertin, J.; Hannemann, J.; Schick, C.; Potter, M.; Dehne, H. *J. Chem. Phys.* **1998**, *108*, 9062.
(21) Sanz, A.; Jiménez-Ruiz, M.; Nogales, A.; Martín y Marero, D.; Ezquerra, T. A. *Phys. Rev. Lett.* **2004**, *39*, 015503.
(22) Jiménez-Ruiz, M.; Ezquerra, T. A.; Sics, I.; Fernández-Díaz, M. T. *Appl. Phys. A* **2002**, *74*, S543.
(23) Shafee, E. El. *Eur. Polym. J.* **2001**, *37*, 1677.
(24) Fukao, K.; Miyamoto, Y. J. *J. Non-Cryst. Solids* **1997**, *212*, 208. Fukao, K.; Miyamoto, Y. J. *J. Non-Cryst. Solids* **1998**, *235−237*, 534.
(25) Mierzwa, M.; Floudas, G. *IEEE Trans. Dielectrics EI* **2001**, *8*, 359. (Reproduced in Floudas, G. Effect of pressure on the dielectric spectra of polymeric systems. In *Broadband Dielectric Spectroscopy*; Kremer, F., Schönhals, A., Eds.; Springer Verlag: Berlin, 2003; chapter 8.)
(26) Cerveny, S.; Zinck, P.; Terrier, M.; Arrese-Igor, S.; Alegría, A.; Colmenero, J. *Macromolecules* **2008**, *41*, 8669.
(27) Avrami, M. *J. Chem. Phys.* **1939**, *7*, 1103; **1940**, *8*, 212; **1941**, *9*, 177.
(28) Mansour, A. A.; Saad, G. R.; Hamed, A. H. *Polymer* **1999**, *40*, 5377.
(29) Madbouly, S. A.; Mansour, A. A.; Abdou, N. Y. *Eur. Polym. J.* **2007**, *43*, 3933.
(30) Hu, Y. S.; Rogunova, M.; Schiraldi, D. A.; Hiltner, A.; Baer, E. *J. Appl. Polym. Sci.* **2002**, *86*, 98.
(31) Avramov, I.; Avramova, K.; Russel, C. *J. Cryst. Growth* **2005**, *285*, 294.
(32) Napolitano, S.; Wubbenhorst, M. *J. Non-Cryst. Solids* **2007**, *353*, 4357.
(33) Affouard, F., *Private communication*. The estimation of the dipolar moment was accomplished by using Gaussian98 [Frisch M. J. *Gaussian 98*, Revision A.11.1; Gaussian, Inc.: Pittsburgh PA, 2001]. Base: B3LYP/6-31G*.
(34) Massalska-Arodz, M.; Williams, G.; Smith, I. K.; Conolly, C.; Aldridge, G. A.; Dabrowski, R. *J. Chem. Soc., Faraday Trans.* **1998**, *94*, 387.
(35) Brás, A. R.; Noronha, J. P.; Antunes, A. M. M.; Cardoso, M. M.; Schönhals, A.; Affouard, F.; Dionísio, M.; Correia, N. T. *J. Phys. Chem. B* **2008**, *112*, 11087.
(36) Havriliak, S.; Negami, S. *Polymer* **1967**, *8*, 161. Havriliak, S.; Negami, S. *J. Polym. Sci. C* **1966**, *16*, 99.
(37) Schönhals, A.; Kremer, F. Analysis of Dielectric Spectra. In *Broadband Dielectric Spectroscopy*; Kremer, F., Schönhals, A., Eds.; Springer Verlag: Berlin, 2003; Chapter 3.
(38) Soccio, M.; Nogales, A.; Lotti, N.; Munari, A.; Ezquerra, T. A. *Polymer* **2007**, *48*, 4742.
(39) Lund, R.; Alegría, A.; Goitandía, L.; Colmenero, J.; González, M. A.; Lindner, P. *Macromolecules* **2008**, *41*, 1364.
(40) Fukao, K.; Miyamoto, Y. *Phys. Rev. Lett.* **1997**, *79*, 4613.
(41) Doremus, R. H. *Rates of Phase Transformations*; Academic: Orlando, 1985.
(42) Gutzow I.; Schmelzer, J. *The Vitreous State: Thermodynamics, Structure, Rheology, and Crystallization*; Springer-Verlag: Berlin, 1995.
(43) Meares, P. *Polymers, Structure and Bulk properties*; Van Nostrand: London, 1965. Cowie, J. M. G. *Polymers, Chemistry and Physics of Modern Materials*; Blackie: Glasgow, 1991 (quoted in ref 15).
(44) Kolmogorov, A. *Izv. Acad. Sci. USSR, Ser. Math.* **1937**, *1*, 355 (quoted in ref 31).
(45) Andjelić, S. A.; Fitz, B. D. *J. Polym. Sci., Part B: Polym. Phys.* **2000**, *38*, 2436.
(46) Brás, A. R.; Malik, P.; Dionisio, M.; Mano, J. F. *Macromolecules* **2008**, *41*, 6419.

JP903212G